MATERIALS SCIENCE

# The surface stress of biomedical silicones is a stimulant of cellular response

**Zhu Cheng[1], Carolyn R. Shurer[1], Samuel Schmidt[1,2], Vivek K. Gupta[3,4], Grace Chuang[1], Jin Su[5], Amanda R. Watkins[5], Abhishek Shetty[6], Jason A. Spector[7], Chung-Yuen Hui[3,8], Heidi L. Reesink[5], Matthew J. Paszek[1,2,9,10]***



**Silicones are commonly used for lubrication of syringes, encapsulation of medical devices, and fabrication of surgical implants. While silicones are generally viewed as relatively inert to the cellular milieu, they can mediate a variety of inflammatory responses and other deleterious effects, but the mechanisms underlying the bioactivity of silicones remain unresolved. Here, we report that silicone liquids and gels have high surface stresses that can strongly resist deformation at cellular length scales. Biomedical silicones, including syringe lubricants and fillings from FDA-approved breast implants, readily adsorb matrix proteins and activate canonical rigidity sensing pathways through their surface stresses. In 3D culture models, liquid silicone droplets support robust cellular adhesion and the formation of multinucleated monocyte-derived cell masses that recapitulate phenotypic aspects of granuloma formation in the foreign body response. Together, our findings implicate surface stress as a cellular stimulant that should be considered in application of silicones for biomedical purposes.**

## INTRODUCTION

Silicones are broadly used for biomedical applications because of their ease of molding (*1*), tunable mechanical properties (*2*), long usage history, and ability to be functionalized with additional chemistry (*3*). Silicone gels are by far the most popular implant material for cosmetic and reconstructive procedures with about 370,000 silicone devices implanted in the United States for breast reconstruction and augmentation alone in 2017 (*4*). While silicones have long been regarded as biocompatible and safe, rare but serious diseases, including multiple types of lymphoma, are linked to silicone implants. For instance, breast implant–associated anaplastic large cell lymphoma (BIA-ALCL) appears primarily in patients with implants having textured silicone surfaces (*5*). A more common complication of reconstructive and aesthetic breast surgeries is capsular contraction, a local response thought to occur because of an excessive fibrotic foreign body reaction to the silicone of implants (*6*). Large silicone granulomas in the breast and lymph nodes are also commonly reported in patients following rupture of breast implants, current generations of which fail at rates of 10 to 14% (*7*, *8*). While foreign body reactions are common responses to silicone gels, the underlying mechanisms remain unclear.

Beyond their application in implantable materials, silicones are also commonly used for lubrication of biomedical devices. Notably, the pharmaceutical and health care industries are increasingly adopting prefilled syringes as an alternative to traditional vial packaging for injectables (*9*). Prefilled syringes are often constructed with glass barrels and lubricated with liquid silicone oils to ensure a smooth gliding behavior of the plunger within the barrel (*9*). Coincident with the adoption of prefilled syringes, medical case reports that describe silicone oil droplets in patients following drug administration have surged (*10*). Reports indicate that prefillable syringes can generate more than 200,000 visible silicone particles per milliliter of injected formulation (*11*). For patients with diabetes who inject themselves daily with insulin, some studies estimate an annual injection of 160 to 270 mg of silicone liquid into the subcutaneous tissue per individual even with traditional vial packaging when administered with lubricated syringes (*9*, *12*). Like silicone gels, injected silicone oils can elicit strong foreign body responses, some of which have been observed more than a decade after the initial injection (*13*). Notably, granulomas composed of macrophages that fuse to form multinucleated giant cells are a well-documented but poorly understood response to injected silicones (*7*, *13*).

Physical directives from natural and synthetic tissue scaffolds can instruct complex cellular and multicellular behaviors, including proliferation (*14*, *15*), differentiation (*16*), migration (*17*), and tissue assembly (*15*). Cells physically probe the rigidity and time-dependent mechanical properties of their extracellular substrate using integrin-based adhesion complexes (*14*, *15*, *18*–*20*). On more rigid substrates, integrin receptors assemble into larger multimolecular complexes that trigger activation of regulatory signaling cascades, a process referred to as rigidity sensing (*14*, *15*). Pathological changes in substrate rigidity can lead to the dysregulation of individual cellular responses and tissue-level behaviors. For instance, increased matrix rigidity is implicated in the progression of fibrosis (*15*, *21*), activation of macrophages and other proinflammatory responses (*22*–*24*), and malignant progression of the breast and other tissues (*25*–*27*). The ability of matrix rigidity to drive these pathological states motivates a consideration of whether materials that are injected or implanted for biomedical purposes could activate rigidity sensing pathways.

Biomedical silicones with negligible or low elasticity are generally assumed to have a minimal capacity to stimulate mechanotransduction. However, all materials have a characteristic surface energy, which is defined as the energy penalty per unit area. In a liquid, this

[1]Robert Frederick Smith School of Chemical and Biomolecular Engineering, Cornell University, Ithaca, NY 14853, USA. [2]Kavli Institute at Cornell for Nanoscale Science, Ithaca, NY 14853, USA. [3]Sibley School of Mechanical and Aerospace Engineering, Cornell University, Ithaca, NY 14853, USA. [4]Department of Mechanical Engineering, Stanford University, CA 94305, USA. [5]College of Veterinary Medicine, Cornell University, Ithaca, NY 14853, USA. [6]Rheology Department, Anton Paar USA Inc., Ashland, VA 23005, USA. [7]Weill Cornell Medicine, Cornell University, New York, NY 10065, USA. [8]Field of Theoretical and Applied Mechanics, Cornell University, Ithaca, NY 14853, USA. [9]Field of Biophysics, Cornell University, Ithaca, NY 14853, USA. [10]Field of Biomedical Engineering, Cornell University, Ithaca, NY 14853, USA.
*Corresponding author. Email: mjp31@cornell.edu

energy penalty gives rise to a uniform surface stress called the surface tension, which is the only means for a liquid to resist deformation. For example, insects such as fishing spiders would not be able to walk on water if not for surface tension at the air-liquid interface. In solids, surface energy also gives rise to surface stresses, and these surface stresses can similarly resist deformation (*28*). In isotropic solids that have uniform mechanical properties, the surface stress is an isotropic tensor determined by a single parameter, $\gamma$. Like liquids, this parameter is often referred to as the surface tension of the solid.

Recent studies have illustrated that solid surface tension can have a dominant role in the mechanical behavior of soft materials when the size of a deforming object is comparable to or smaller than the elastocapillary length, which is the ratio of the material's surface tension to its elasticity, $\gamma/E$, where $E$ is the Young's modulus (*28*–*30*). For soft silicones, elastocapillary lengths on the micrometer scale have been observed (*29*), suggesting that surface tension might provide an appreciable resistance to deformation at cellular and subcellular length scales. Here, we consider whether the surface stresses of silicones can activate rigidity pathways to modulate downstream cellular responses. Our studies consider biomedical silicones, liquid silicone oils, and model silicone gel systems of varying bulk rigidity.

## RESULTS

### Rigidity sensing on biomedical silicone gels and model materials

We evaluated the response of cells to soft silicone gels that we extracted from fourth- and fifth-generation implantable devices currently approved by the U.S. Food and Drug Administration for breast reconstruction and augmentation. The silicone fillings were extracted through a puncture site in the outer shell of each implant and spread on the bottom of cell culture dishes. The filling of the fourth-generation device was a viscous silicone gel, whereas the fifth-generation filling was a more cohesive gel that is commonly referred to in clinical practice as a "form-stabilized" or "gummy bear" silicone (*31*). The extracellular matrix (ECM) protein fibronectin, which is abundant in plasma and other body fluids, readily adsorbed to the surface of the gels without any surface treatments or coupling reagents (fig. S1A). Mammary epithelial cells (MECs) plated on the soft gel extracts were well spread with a polygonal morphology (Fig. 1A). Induction of cell spreading on the soft biomedical silicones was unexpected on the basis of prior observations that cell spreading responses are suppressed on highly compliant substrates because of insufficient stimulation of rigidity sensing pathways (*14*, *16*, *17*).

To better characterize rigidity sensing responses to silicone biomaterials, we took advantage of a model silicone gel system of tunable elasticity (*32*). Notably, we did not oxidize the silicone substrates with treatments such as gas plasma or ultraviolet (UV)/ozone since these procedures are known to form a rigid silica layer on the gel surface. Fibronectin readily adsorbed to the unmodified surfaces of silicone gels (fig. S1A). The cells on both soft and stiff silicone substrates were highly spread (Fig. 1A) and exhibited well-formed actin arcs, longitudinal stress fibers, and focal adhesions with $Tyr^{397}$ phosphorylated focal adhesion kinase ($FAK^{pY397}$), a marker of active rigidity signaling (Fig. 1B and fig. S2). We confirmed that the soft gel extracts from fourth- and fifth-generation breast implants also stimulated activation of $FAK^{pY397}$ (Fig. 1C). As a control, we evaluated cellular responses on polyacrylamide (PA) gels that were of comparable elastic moduli to the silicone gels and were conjugated with similar surface levels of fibronectin (fig. S1). In these studies, we assumed that both silicone and PA gels were incompressible, and thus, their bulk stiffness was described by a single parameter, $E$ (*33*, *34*). As expected, cells on the soft PA substrates were not mechanically activated, as indicated by their poorly spread morphology, lack of discernable actin bundles, and low levels of $FAK^{pY397}$ (Fig. 1A and fig. S2). We confirmed that mouse and human fibroblasts, which are typically more contractile than epithelial cells, responded similarly to the silicone gels (fig. S3).

We next tested whether rigidity signaling by silicones was linked functionally to transcriptional regulation. The gene regulatory factor Yes-associated protein (YAP) was previously shown to shuttle from the cytoplasm to the nucleus where it complexes with transcriptional coactivator with PDZ-binding motif (TAZ) to turn on gene expression when rigidity sensing pathways are activated (*35*). Notably, cells on soft silicone gels, including extracts from breast implants, exhibited nuclear YAP levels comparable to cells on rigid substrates. In contrast, YAP was mostly cytoplasmic in cells on soft hydrogels (Fig. 1D and fig. S4A). We confirmed that blocking rigidity signaling through pharmacological inhibition of activated FAK on rigid substrates stunted YAP translocation to the nucleus (fig. S4B) (*36*). Consistent with up-regulated YAP transcriptional responses, expression levels of YAP-dependent connective tissue growth factor (CTGF) and ankyrin repeat domain 1 (ANKRD1) were up-regulated in cells on soft silicones compared to cells on soft hydrogels (fig. S4C). Cell proliferation, previously shown to be induced by YAP/TAZ transcriptional activation (*35*), was also enhanced on soft silicones compared to soft hydrogels (fig. S4, D to G).

We also tested whether silicone materials of vanishingly small elastic modulus, such as the silicone liquids used to lubricate syringes and biomedical devices, could similarly trigger the activation of rigidity signaling pathways. Cells adhered and spread well on liquid silicone oil layers dispensed on the bottom of culture dishes (Fig. 1A). Unexpectedly, silicone liquids were able to stimulate translocation of YAP to the cell nucleus as effectively as rigid cellular substrates (Fig. 1, A and D).

To test whether ligand presentation might explain the ability of silicones to stimulate rigidity responses, we functionalized silicone substrates, as well as control PA gels, with arginine - glycine - aspartic acid (RGD) adhesive peptides that had a single terminal cysteine for chemically defined thiol-maleimide (MAL) linkage to the gels (Fig. 2A and fig. S5). The peptide included a tetramethylrhodamine (TAMRA) fluorophore for assessment of the relative conjugation density of RGD (Fig. 2A and fig. S5). By optimizing the conjugation protocols for each gel system, the adhesive peptides were conjugated uniformly and at similar surface densities on the silicone and PA substrates (Fig. 2, A to C). Similar responses to fibronectin-adsorbed and RGD-conjugated substrates were observed (Fig. 2, B and D). Notably, highly compliant silicone substrates with anchored RGD peptides stimulated cell spreading responses comparable to silicone or hydrogel substrates of much higher rigidity (Fig. 2, B and D).

### Substrate surface tension can dominate in cellular rigidity sensing

We considered whether cells were sensing the surface stress of soft or liquid silicones rather than the bulk elasticity of these materials. We noted that surface stresses arise from the interfacial free energy,

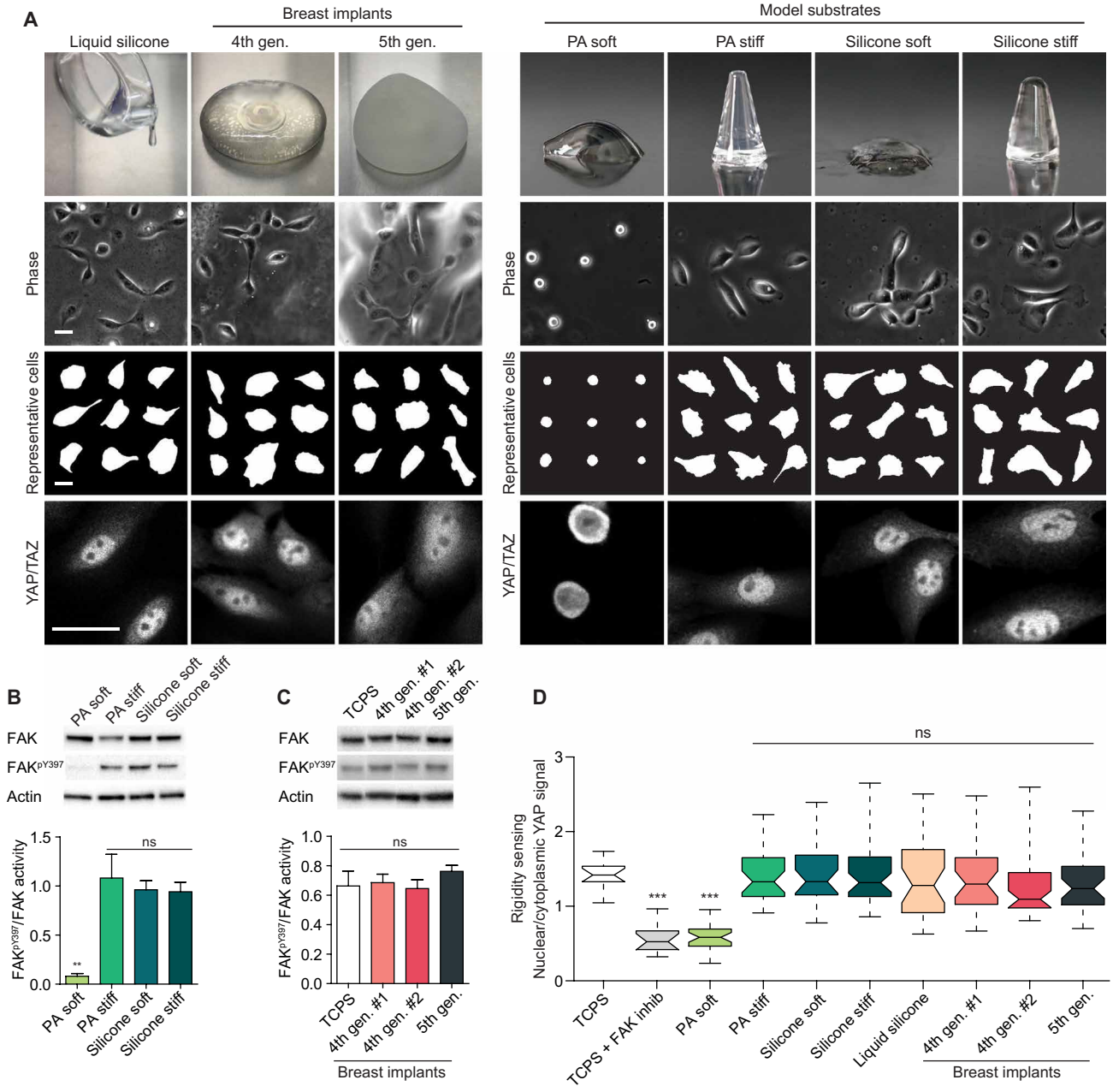


**Fig. 1. Silicone liquids and soft gels stimulate rigidity signaling responses.** (**A**) Top row: Pictures of fourth-generation and fifth-generation breast implants, liquid silicone oil, and soft or rigid polyacrylamide (PA) and silicone gels. Lower rows: Representative phase-contrast images, cell masks, and Yes-associated protein (YAP)/transcriptional coactivator with PDZ-binding motif (TAZ) staining of MCF10A MECs on the indicated substrate with adsorbed fibronectin. Scale bars, 30 μm. Experiments were conducted in triplicate. PA soft, 0.12 kPa; PA stiff, 20 kPa; silicone soft, 0.1 kPa; silicone stiff, 21 kPa; liquid silicone, negligible elasticity. Photo credit: Zhu Cheng and Matthew Paszek, Cornell University. (**B**) Top: Representative immunoblot of total and phospho-FAK in MECs on the indicated substrates. Bottom: Quantification of the ratio of phospho-FAK to total FAK from immunoblot shown in the top panel. Error bars show SEMs. $^{**}P < 0.005$ and ns, not significant [one-way analysis of variance (ANOVA) with Tukey's post hoc test]; $n > 4$. (**C**) Representative immunoblot of total and phospho-FAK in MECs on the indicated substrates (top) and quantification of immunoblot signal (bottom). TCPS, tissue culture polystyrene. Error bars show SEMs. ns, not significant. Wilcoxon rank scores test was used; $n > 4$. (**D**) Quantification of the ratio of nuclear YAP signal to cytoplasmic YAP signal. $^{***}P < 0.001$, one-way ANOVA; $n > 35$ per condition. Experiments were conducted in triplicate. Horizontal lines are medians. Boxes show the interquartile range (IQR). Whiskers extend to minimum and maximum values.

or surface energy, at material interfaces. To evaluate the surface energies of fibronectin-functionalized substrates, we measured the contact angles formed with a liquid water droplet. The functionalized silicone substrates had a considerably higher surface energy in water, as indicated by a significantly reduced wettability (contact angle, 102.6 ± 1.3°; mean ± SEM; fig. S6, A and B), compared to functionalized hydrogel substrates (contact angle, 48.7 ± 9.3°; mean ± SEM; fig. S6, A and B). Surface energy was essentially independent of silicone or hydrogel cross-linking and elastic modulus (fig. S6B).

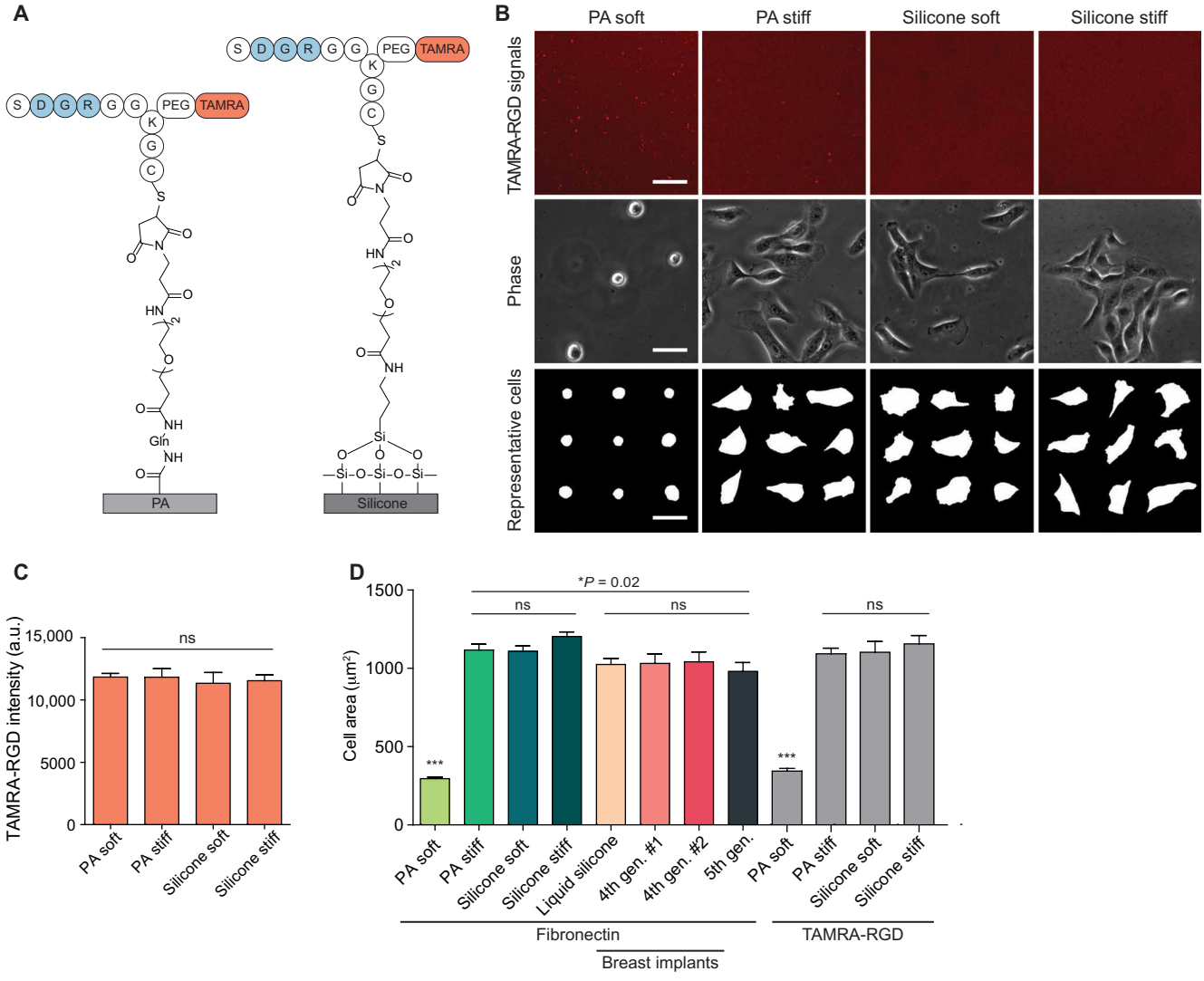


**Fig. 2. Cellular stimulation by silicone is not explained by differences in ligand tethering.** (**A**) Covalently attached TAMRA-tagged RGD peptide on the surfaces of PA and silicone substrates. (**B**) Top: Representative fluorescence images of TAMRA-RGD peptide conjugated on the surface of PA and silicone substrates. Lower rows: Phase-contrast images and representative cell masks of MECs on PA and silicone substrates of the indicated stiffness. Scale bars, 50 μm. (**C**) Quantification of the mean fluorescence intensity of the TAMRA-RGD peptide on soft and stiff substrates. *t* test was used. Five independent samples were used per condition ($n > 20$ per condition). a.u., arbitrary units. (**D**) Quantification of cell spread area of MECs on PA substrates with conjugated fibronectin, silicone substrates with adsorbed fibronectin, and PA or silicone substrates with conjugated TAMRA-RGD peptide. ***$P < 0.001$, *t* test; $n > 45$ cells per condition. PA soft, 0.12 kPa; PA stiff, 20 kPa; silicone soft, 0.1 kPa; silicone stiff, 21 kPa. Experiments were conducted in triplicate. Error bars show SEMs.

To test for the existence of surface stresses in our substrates, we used confocal fluorescence microscopy to measure the indentation of small, spherical steel balls into our gels. The gels were functionalized with fluorescently labeled fibronectin, which served as a marker of the gel surface (Fig. 3, A and B). We coated the surface of the steel balls with a thin nonadhesive polymer coating to minimize adhesion and frictional contact with the substrate surface (fig. S6C and movies S1 and S2). Indentation depth was measured on substrates of bulk elasticity ranging from 0.1 to 4 kPa (Young's modulus), as confirmed by dynamic mechanical thermal analysis (DMTA; fig. S1, C and D). We observed that the surface indentation of soft silicone gels was much smaller than that of PA gels of comparable bulk elasticity (Fig. 3B). We compared these deformations to Hertz contact theory, which originally was developed to describe the indentation of isotropic elastic solids with negligible surface stresses (*37*). PA substrates agreed well with Hertz's prediction that indentation depth should scale with $E^{-2/3}$ (Fig. 3, C and D) (*37*). In contrast, indentation of silicone substrates did not follow the Hertz scaling law, suggesting that a force in addition to elasticity resisted the deformation of these materials (Fig. 3, C and D).

We tested whether surface stress could explain the deviation from Hertz contact theory. Surfactants are known to reduce the surface energy at liquid-liquid and liquid-solid interfaces. With the addition of the surfactant Triton X-100, the indentation of compliant silicone substrates drastically increased (Fig. 3B and fig. S7), strongly suggesting that solid surface tension is non-negligible in the silicone materials. We measured surface hardness to test more

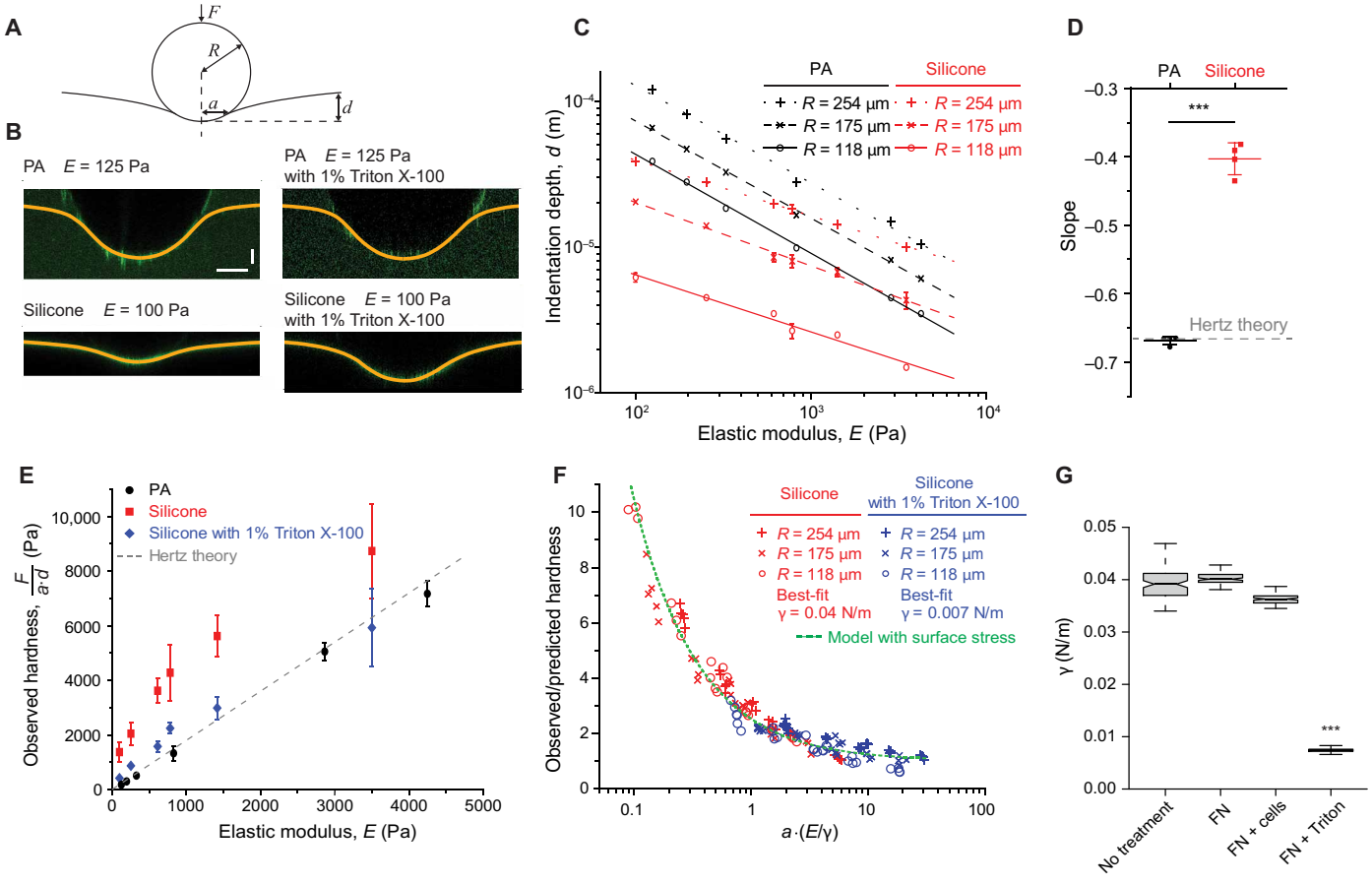


**Fig. 3. Silicone substrates have high surface energies and surface stresses.** (**A**) Schematic depicting the indentation of a rigid indenter (steel ball) into an elastic substrate. (**B**) Confocal fluorescence images showing the surface profiles of PA gels ($E = 125$ Pa; top left) and silicone gels ($E = 100$ Pa; bottom left) submerged in buffer or buffer with 1% Triton X-100 and indented by steel balls with radii of 254 μm. Horizontal scale bar, 100 μm; vertical scale bar, 30 μm. (**C**) Indentation depth, $d$, of the steel ball versus substrate elastic modulus, $E$, for PA and silicone gels of the indicated stiffness. Steel balls used were 254, 175, or 118 μm in radii, as indicated; $n \geq 5$. (**D**) Slopes of the log-log scale plots shown in (C). Hertz contact theory predicts a slope of −2/3. ***$P < 0.001$, $t$ test; $n = 4$. Error bars show SEMs. (**E**) Observed substrate hardness, $F/(a{\cdot}d)$, versus elastic modulus; $F$ is the indentation force, and $a$ is the measured contact radius of the indenter. The dashed line shows the prediction by Hertz contact theory; $n \geq 12$. Error bars show SEMs. (**F**) Ratio of observed and predicted hardness, $(a^*{\cdot}d^*)/(a{\cdot}d)$, versus the elastocapillary number, $a{\cdot}(E/\gamma)$, for silicone gels submerged in buffer or buffer with surfactant. $a^*$ and $d^*$ are the Hertz predicted contact radius and indentation depth, respectively. Experimental data converge on a theoretical model of contact for an elastic substrate having surface tension. Best-fit surface tensions are 0.04 and 0.007 N/m for measurements in buffer and buffer with surfactant, respectively. (**G**) Best-fit surface tensions of silicone substrates with no adsorbed surface proteins (No treatment), adsorbed with fibronectin (FN), adsorbed with fibronectin and measured after 24 hours of culture with MEC cells (FN + cells), or adsorbed with fibronectin and treated with 1% Triton X-100 (FN + Triton). ***$P < 0.001$, $t$ test; $n \geq 100$. Horizontal lines are medians. Boxes show the IQR. Whiskers extend to minimum and maximum values.

specifically whether surface tension resists the deformation. Hardness provides a relationship between indentation force, $F$, and deformation, $d$, and is defined as $F/(a{\cdot}d)$, where $a$ is the contact radius of the indenter with the substrate. The observed hardness for PA gels again matched expectations based on Hertz contact theory for isotropic elastic solids. In contrast, the observed hardness of the silicone substrates was significantly greater than Hertz's prediction (Fig. 3E). We next compared our experimental measurements to theoretical predictions based on a contact theory that includes a treatment of surface stresses (*28*, *38*). This theory predicts that deviation of hardness from classical Hertz theory depends on a single dimensionless quantity, the elastocapillary number ($a{\cdot}E/\gamma$) (fig. S6D). Thus, if surface stresses account for the increase in apparent hardness of silicone substrates, then the hardness for different indenter radii and different substrate elastic moduli should converge on a single curve when plotted against the elastocapillary number. Figure 3F shows that this was indeed the case.

By fitting the experimental data to the contact model, we found that our silicone substrates have a surface tension of 0.04 N/m in water and 0.007 N/m in water plus Triton X-100 surfactant (Fig. 3F and fig. S7). We repeated the indentation tests before and after cells were cultured on the substrates and confirmed that prolonged cell culture did not significantly alter the surface tension of silicone substrates (Fig. 3G and fig. S8). We also confirmed that fibronectin adsorption did not significantly alter the surface stresses (Fig. 3G and fig. S9). The model and experimental measurements indicated that the surface tension of silicones would dominate over their bulk elasticity for elastocapillary numbers of approximately unity or smaller. Since the effective hardness depends on a single dimensionless quantity (Fig. 3F), we could estimate the resistance encountered

by a deforming body of any arbitrary size. For a cell with a typical diameter of 20 μm, our measurements indicate that surface stresses should become dominant in the deformation of silicone substrates when their elastic modulus is less than ~2 kPa (Fig. 4A). Consistent with expectations based on this simple scaling argument, we observed essentially no dependence of cell spreading on substrate elasticity for silicones with elastic moduli less than ~1 to 2 kPa (Fig. 4A).

We tested whether a biocompatible surfactant could attenuate the induction of cell spreading on soft silicone materials. After testing a variety of commercially available surfactants, we found that the nonionic surfactant Span 85 markedly reduced the solid surface tension of our silicone substrates and had no significant effect on cell viability after 24 hours of culture (Fig. 4, B and C). Notably, Span 85 treatment mitigated the ability of soft silicones to stimulate cell spreading. The treatment had no significant effect on the spreading of cells on rigid substrates, consistent with elasticity being the dominant mechanostimulatory cue from these rigid materials (Fig. 4D). Notably, the surfactant could not penetrate the silicone gels and, therefore, would not be expected to change the bulk viscoelastic properties and network structure of the silicone gels. Hence, our results argued against stress relaxation (*19*, *20*), creep compliance (*39*, *40*), and porosity (*41*) as alternative explanations for the ability of soft silicone gels to stimulate the cell-spreading response. Instead, our results strongly implicated solid surface stress as the primary stimulatory cue for liquid silicones and highly compliant gels.

### Liquid silicone oils stimulate foreign body–like responses in biomimetic tissue platforms

As a functional test, we considered how peripheral blood mononuclear cells (PBMCs) might interact with polydimethylsiloxane (PDMS) oil, which is the most common syringe lubricant. We found that PDMS oil readily adsorbed fibronectin from aqueous solutions (Fig. 5A). We conducted rheological measurements of the interface between silicone oil and physiological buffer on a rotational rheometer with a biconical disk–based measuring system. The elasticity of the silicone oil–water interface built up over time, with the interfacial storage modulus reaching a very stiff plateau of approximately 0.3 N/m (fig. S10A). Adsorption of fibronectin did not appreciably affect the elasticity of the interface (fig. S10A). The interfacial loss modulus was negligible, indicating that the interface had a nearly purely elastic response to stress (fig. S10A). To recapitulate the retention of silicone oil droplets in injected tissues, we created a biomimetic culture platform where silicone oil was coated on culture dishes and overlaid with collagen gels or where silicone oil microdroplets were dispensed from a syringe needle and fully encapsulated in three-dimensional (3D) collagen gels (Fig. 5B and fig. S10B).

In the overlay system, equine PBMCs assembled at the silicone oil and collagen gel interface and fused to form giant multinucleated cells. The giant cells contained distinct bands of actin-containing podosomes, which are a characteristic of multinucleated cells in granulomatous tissue and foreign body reactions to implanted biomaterials (Fig. 5C) (*42*). Notably, no inflammatory cytokines were added to the culture media, indicating that exogenous cytokines were not necessary for giant cell formation or podosome assembly. Rigid glass substrates overlaid with collagen gels similarly supported giant cell formation (Fig. 5, C and D). However, attenuation of rigidity signaling by pharmacological inhibition of FAK or Src drastically reduced the number of multinucleated cells (Fig. 5D).

We next investigated the interaction between PBMCs and 3D silicone microdroplets. Silicone liquids were coexpelled with culture media from a standard syringe barrel by the force of the plunger and gelled in collagen gels to suspend microdroplets (Fig. 5E and fig. S10B). Mononuclear-derived cells migrated through the 3D collagen matrices and engaged the silicone microdroplets (Fig. 5F). We observed the formation of large, multinucleated cells that formed single cup-like structures wrapping around the silicone droplets, indicating a strong adhesive interaction between cells and the silicone droplet (Fig. 5F). The multinucleated cells displayed surface markers for major histocompatibility complex II (MHCII), which is a marker of macrophages and dendritic cells that give rise to granulomatous tissue during foreign body responses in vivo (Fig. 5F) (*43*, *44*).

## DISCUSSION

Together, our results reveal material surface stress as a potent mechanostimulant that can modulate diverse biological behaviors. While

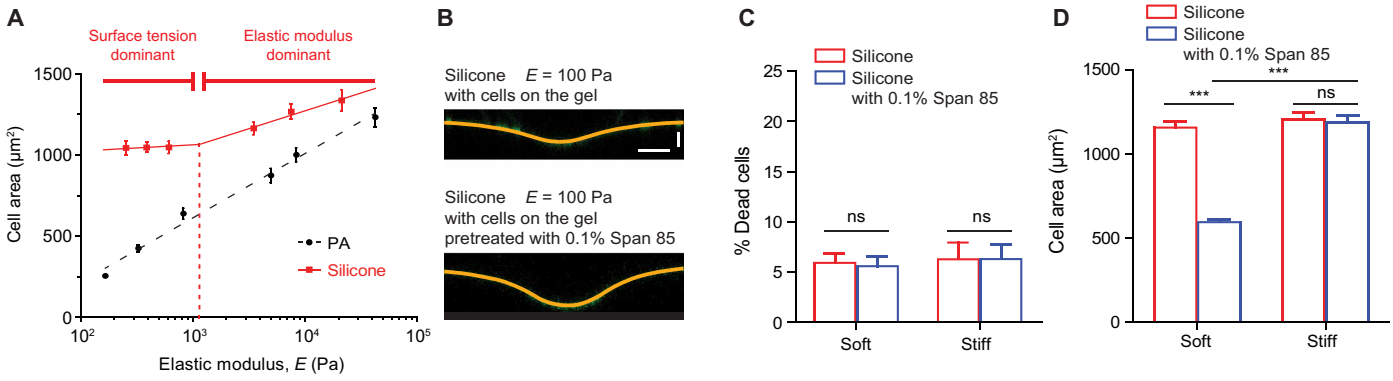


**Fig. 4. Surfactant treatment reduces silicone surface stresses and attenuates rigidity responses.** (**A**) Relationships between cell spread area of MECs and the elastic moduli of PA or silicone gels; $n > 40$ cells per condition. Experiments were conducted in triplicate. (**B**) Confocal fluorescence images showing the indentation profiles of silicone gels with or without pretreatment with surfactant (0.1% Span 85). Indentation measurements were made using 254-μm radius steel balls after culture of cells for 24 hours. Horizontal scale bar, 100 μm; vertical scale bar, 30 μm. (**C**) Percentage of dead cells among total cells growing on silicone gels versus surfactant (0.1% Span85)–pretreated silicone gels 24 hours after seeding. *t* test was used. A total of 190 to 280 cells were analyzed for each condition. Experiments were conducted in triplicate. (**D**) Quantification of cell area on silicone gels versus surfactant (0.1% Span85)–pretreated silicone gels. ***$P < 0.001$, *t* test; $n \geq 40$. Experiments were conducted in triplicate. Error bars show SEMs.

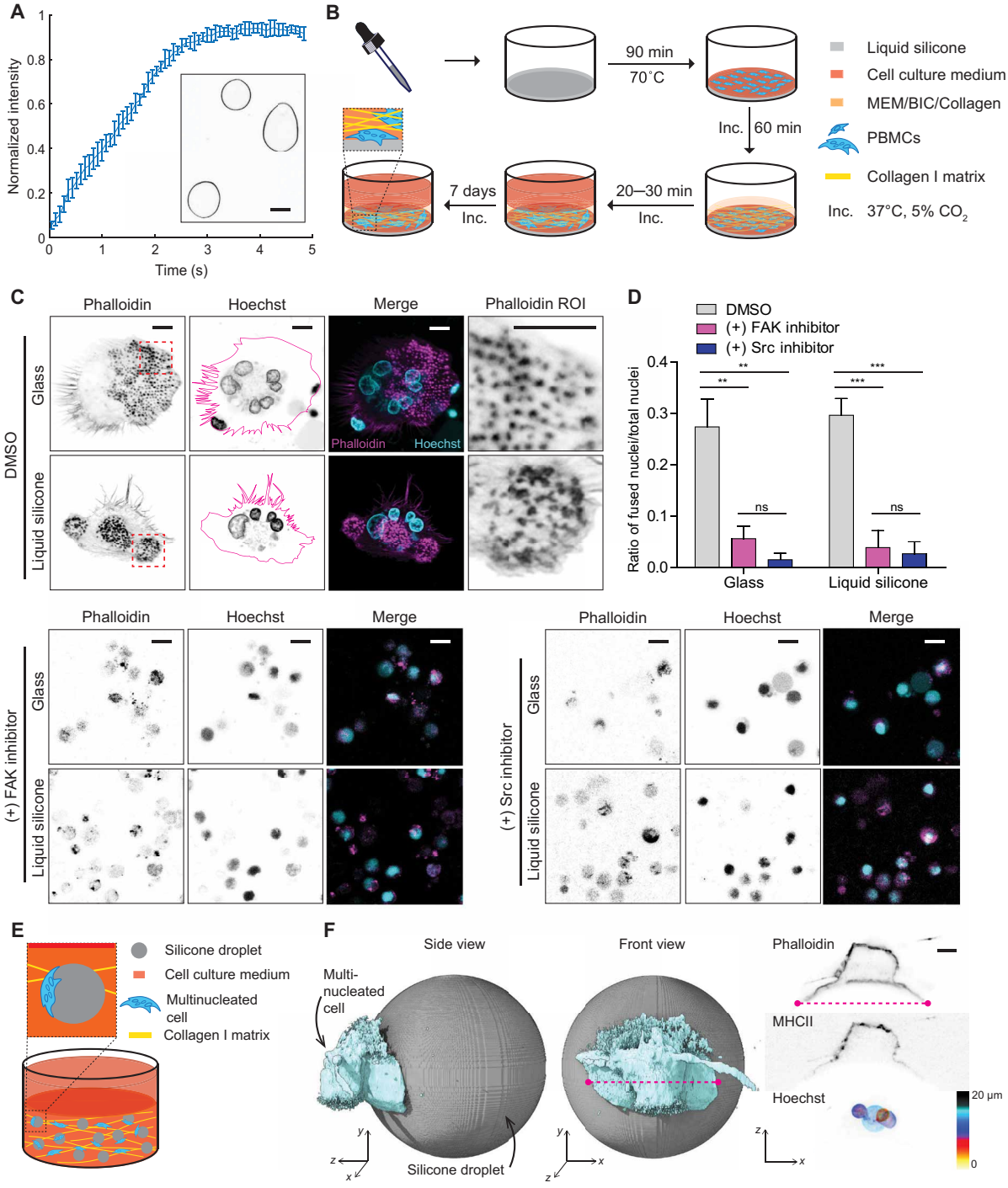


**Fig. 5. Silicone stimulates foreign body–like responses.** (**A**) Kinetics of fibronectin adsorption onto silicone droplets. Inset: Confocal images of adsorbed ATTO 488-fibronectin on the surface of silicone droplets. Scale bar, 10 µm. (**B**) A schematic workflow for silicone-collagen overlay assays with PBMCs. Silicone oil was spread on the bottom of 96-well plates and incubated as indicated. Subsequently, PBMCs were seeded on top of the silicone and allowed to adhere before covering the cells with bovine collagen I solution. After polymerization of the collagen, samples were placed in an incubator and cultured for 7 days at 37°C, 5% $CO_2$. MEM, minimal essential Eagle's medium; BIC, sodium bicarbonate. (**C**) Representative images of the cells on glass and silicone substrates overlaid with collagen and treated with dimethyl sulfoxide (DMSO) control, 5 µM PF-573228 (FAK inhibitor), and 0.1 µM dasatinib (Src inhibitor). Dashed red squares in the first column panels designate regions of interest (Phalloidin ROI). Scale bars, 8 µm. PBMCs from two independent horse donors were tested in triplicate. (**D**) Ratio of the number of nuclei from the fused multinucleated foreign body–like giant cells over total number of nuclei. Cells from two different horse donors were analyzed. More than 110 nuclei were analyzed for each horse per condition. ***$P < 0.001$ and **$P < 0.01$, *t* test. Error bars show SEMs. (**E**) Schematic depicting the interaction of multinucleated foreign body–like giant cells with silicone droplets. (**F**) 3D reconstruction of PBMCs on the spherical silicone droplet. Blue, multinucleated foreign body giant cell; gray, silicone droplet. Left: side view; middle: front view; right: immunofluorescence images of filamentous actin stained with phalloidin and major histocompatibility complex II (MHCII) in PBMC clusters on the silicone droplet and a *z* projection of cell nuclei in the cluster. PBMCs from two independent horse donors were tested in triplicate. Scale bar, 5 µm.

silicones are generally considered to be biologically inert, their ability to adsorb matrix proteins and provide mechanostimulatory cues confers an unexpected bioactivity to these materials. Even liquid silicones, such as those used for syringe lubrication, could activate rigidity-associated responses. Substrate stiffness (*15*, *45*), stress relaxation (*19*, *20*), creep compliance (*39*, *40*), porosity (*41*), and ligand tethering (*45*, *46*) are all previously reported attributes that cells can sense and respond to. The current work adds surface stress to the known list of ECM parameters that can physically direct cell responses.

Further investigation is required to determine what role, if any, mechanical stimulation by surface stresses contributes to silicone-associated pathologies, including inflammation; granuloma formation; fibrotic capsule assembly; and rare diseases, such as BIA-ALCL (*4*). Nevertheless, our in vitro studies clearly implicate surface stress as a potent mechanostimulant of integrin signaling; YAP/TAZ-mediated gene expression; and downstream cellular responses, including changes in cell morphology. A growing body of evidence has implicated activation of rigidity sensing pathways in the induction of inflammation, fibrosis, angiogenic outgrowth, and cancer progression (*22*–*24*, *27*, *47*). Substrate rigidity can also directly activate macrophages and induce proinflammatory cytokine production (*22*–*24*), which are key steps in granuloma formation. These observations, when considered in the context of our current findings, motivate a deeper investigation of a possible physical basis for silicone-associated pathologies. For instance, future studies are advised to consider whether rigidity responses to the silicone shell of an implant may contribute to capsular contraction, which remains the most common significant complication of implants (*6*).

Recent advancements in packaging and implant technologies have the potential to significantly reduce patient exposure to silicone oils and viscous gels. Silicone-lubricated syringes remain the most widely used injection system primarily because of their lower cost, legacy approvals, and longer usage history (*9*). However, our results indicate that injected silicone oil droplets could have unexpectedly stiff interfaces with aqueous bodily fluids and may trigger mechanical cell responses. Prefillable syringe systems that are free of silicone lubricants have been developed and are now widely available (*9*). While primarily developed to improve the stability of protein formulations by reducing adsorption to silicone oil droplets, these syringes would essentially eliminate the inadvertent coinjection of silicone oils.

In conclusion, our findings indicate that the surface stresses of materials can be highly effective in activating rigidity sensing pathways. Tuning surface stresses could be a viable strategy for controlling the nano- to microscale deformability of compliant biomaterials and for directing cellular functions. For example, we have found that simple surfactant treatments can reduce the surface stresses of silicone gels and attenuate their physical stimulation of cells. Antifouling coatings on silicone materials might also prevent protein adsorption, cell adhesion, and mechanotransduction. Given that surface stress can dominate in the deformation of highly compliant materials and override directives related to bulk elasticity, our results support additional consideration of surface stress in the design and application of silicones and other materials for medical devices.

## MATERIALS AND METHODS

### Experimental design

Responses of cell lines and primary monocytes to hydrogel and silicone materials in standard cultures or in biomimetic 3D collagen gel systems were analyzed. Hydrogel and silicone substrates were physically characterized and mechanically tested. Mechanical responses were compared with contact models for homogeneous elastic substrates and elastic substrates with surface tension. Pharmacological treatments and surfactants were used to test possible mechanisms of action.

### Gel fabrication

To prepare silicone gels, parts A and B of QGel 310 (Quantum Silicones) were mixed in various ratios ranging from 1:0.60 to 1:8.9 in a Thinky planetary mixer and then degassed for 15 min. The mixtures were cured at room temperature for 1 hour and baked at 60°C for 21 hours. To prepare silicone oils, parts A and B of the aforementioned kit were mixed in the ratio of 1:0.20 in a Thinky planetary mixer and degassed for 15 min. The mixtures were left at room temperature for 1 hour and baked at 60°C for 21 hours. The mixture remained in liquid form because of the low percentage of cross-linking reagent part B. To make PA hydrogels, glass-bottom dishes were activated using 2% 3-aminopropyltriethoxysilane, followed by 0.5% glutaraldehyde to facilitate PA gel attachment to the glass. Top coverslips were treated with Sigmacote to ensure detachment of PA gels. PA solutions with acrylamide at final concentrations of 3 or 7.5% and bis-acrylamide at final concentrations ranging from 0.035 to 0.35% were mixed. *N*,*N*,*N*′,*N*′-tetramethylethylenediamine was added to a final concentration of 0.01% in solution. The PA solution was degassed for 30 min, and ammonium persulfate was added to a final concentration of 0.01% to initiate the polymerization. PA solution was sandwiched between the activated glass-bottom dish and the Sigmacote-treated coverslip and left to polymerize for 20 to 30 min. The top coverslip was then removed, and the polymerized PA gel was submerged in distilled water.

### Gel functionalization with fibronectin

PA gels were functionalized with fibronectin using the cross-linker 6-((acryloyl)amino)hexanoic acid succinimidyl ester (Acryloyl-X SE; Thermo Fisher Scientific). The PA gel functionalization was adapted from a previous protocol (*48*). Briefly, desired amounts of 0.2% bis-acrylamide, 3% Irgacure 2959, 0.5 M Hepes (pH 6.0), and 0.3% Acryloyl-X SE were mixed and applied onto gels. Gels were overlaid with Sigmacote-treated coverslips and then placed under a UV source to activate photoinitiator for 10 min. The top coverslips were removed, and the gels were gently washed with 50 mM Hepes buffer (pH 6) for 5 min on ice three times. The gel substrates were then incubated in fibronectin (20 μg/ml) in 50 mM Hepes buffer (pH 8) overnight at 4°C. The PA gels were washed with phosphate-buffered saline (PBS). For silicone gel functionalization, the cured silicone gels were incubated in fibronectin (10 μg/ml) in PBS overnight at 4°C to allow fibronectin adsorption onto the gels and then washed with PBS.

### Gel functionalization with TAMRA-RGD peptide

The RGD-containing peptide, Ser–Asp–Gly–Arg–Gly–Gly–Lys($PEG_3$-TAMRA)–Gly–Cys was synthesized by AnaSpec. A polyethylene glycol ×3 ($PEG_3$) spacer linked the peptide's lysine to the TAMRA dye. Succinimidyl ester–functionalized PA gels were prepared with Acryloyl-X SE as described above. Gels were next functionalized with amines by incubation overnight with 200 mM glutamine solutions in 50 mM Hepes buffer (pH 8) at 4°C. Functional MAL groups were introduced through MAL-$dPEG_2$-NHS (*N*-hydroxysuccinimide)

ester (Quanta Biodesign) coupling. PA soft gels ($E$ = 140 Pa) were incubated in 2 mM MAL-dPEG$_2$-NHS ester dissolved in 1:1 dimethyl sulfoxide (DMSO):PBS solution, and PA stiff gels ($E$ = 22,000 Pa) were incubated in 0.5 mM MAL-dPEG$_2$-NHS ester dissolved in 1:1 DMSO:PBS solution, both at room temperature for 2 hours. Last, gels were coupled with 10 μM TAMRA-RGD by incubation at room temperature for 2 hours on a shaking platform. Between each chemical treatment, the gels were rinsed with PBS. Silicone gels were functionalized by treatment with 0.95% 3-aminopropyltriethoxysilane in methanol for 5 to 10 min, followed by rinsing with methanol and water and then baking the gels at 60°C for 1 hour. The amine-functionalized gels were coupled with 5 mM MAL-dPEG$_2$-NHS ester in 1:1 DMSO:PBS solution and then 10 μM TAMRA-RGD, as described for PA gels.

### Silicone breast implant–derived materials

Silicone implants were gifts from Mentor Worldwide LLC. The fourth generation (catalog numbers 6580031 and 7333875) and fifth generation (catalog number CPG323) of implants were tested. Implants were cut open with razor blades. The interior materials were pinched with tweezers and spread onto glass-bottom dishes. The gels were functionalized by adsorption of fibronectin at 10 μg/ml in PBS in a 4°C refrigerator overnight. Cells were seeded at 5000 cells/cm$^2$ and analyzed 24 hours after seeding.

### Mechanical characterization

The elastic moduli of PA and silicone gels were measured by DMTA on a Q800 system (TA Instruments). PA gels were cast into Teflon molds of 10 mm in diameter and 3.5 mm in depth between two Sigmacote-treated cover glasses. Silicone gels were cast into agarose molds of 10 mm in diameter and ~3.8 mm in depth and cured as above. Mechanical tests were conducted by compressing the gel samples between two compression clamps along the axes of cylindrical samples with forces slowly ramping up. Vegetable oil was used between gel samples and compression clamps to prevent adhesion. Elastic moduli were calculated from the slope of the stress-strain curves from 7.5 to 12.5% strain. The storage moduli and loss moduli of silicone gels were measured using a DHR3 rheometer (TA Instruments). Silicone gels were cast in molds that were 20 mm in diameter and 2 mm in thickness and cured as above. Samples were loaded between two parallel plates and then sheared by the parallel plates at a frequency of 6.3 rad/s.

### Interfacial rheology measurements

A standard rotational rheometer MCR 302 (Anton Paar) equipped with a Peltier temperature device (P-PTD 200/80I) was used. Temperature was set to 25°C for all measurements. A biconical disk–based measuring system (BiC68-5) in conjunction with an Interfacial Rheology System cell was used to measure the interfacial moduli. A normal force assisted surface detection methodology was used to position the bicone geometry accurately at the buffer-silicone oil interface. A special interfacial analysis software package based on the unique solution of the full flow field for a biconical geometry (*49*) was used for the calculation of the absolute interfacial rheological properties.

### Contact angle measurements

Measurements of water contact angle were conducted on a VCA Optima Contact Angle system (AST Products). Water droplets (1.5 μl) were applied onto fibronectin-coated PA and silicone substrates.

### Steel ball indentation measurements

PA and silicone gels were cast in glass-bottom dishes at a thickness of 500 μm and functionalized with fibronectin previously labeled with ATTO 488-NHS ester according to the manufacturer's protocol (ATTO-TEC GmbH). Steel balls of 254, 175, and118 μm in radii (Abbott Ball Company) were coated with hydrophilic coatings (Coatings2Go) following the manufacturer's protocol to minimize ball-substrate adhesion. Substrates coated with ATTO 488-labeled fibronectin were submerged in PBS and then indented by the steel balls. Surfactant-treated substrates were prepared by incubating the substrates with 1% Triton X-100 at room temperature for 1 hour, followed by five rinses with PBS before measurement. For indentation measurements of substrates with cultured cells, gels seeded with MCF10A cells at 5000 cells/cm$^2$ and cultured for 24 hours before indentation measurements in media. For indentation measurements of substrates without adsorbed fibronectin, gels were submerged in PBS with free ATTO 488 dye to provide contrast for imaging. Gel surface profiles were visualized by taking $z$ stack images of ATTO 488-conjugated fibronectin or ATTO 488 PBS at the indented gel-buffer interface using a Zeiss LSM 880 confocal inverted microscope (i880) with a 10×, 0.45-NA (numerical aperture) objective.

### Gel preparation with Span85 surfactant treatment for cellular assays

To study cellular responses to substrates with reduced surface stresses, silicone substrates were treated with 0.1% (v/v) Span85 aqueous solution at room temperature for 30 min, followed by 10 rinses with PBS. MCF10A cells were then seeded at 5000 cells/cm$^2$ and analyzed 24 hours after seeding.

### Cell lines and culture

MCF10A cells (American Type Culture Collection) were cultured in Dulbecco's modified Eagle's medium (DMEM)/F12 media (Thermo Fisher Scientific) supplemented with 5% horse serum (Thermo Fisher Scientific), epidermal growth factor (EGF; 20 ng/ml; PeproTech), insulin (10 μg/ml; Sigma), hydrocortisone (500 ng/ml), and cholera toxin (100 ng/ml; Sigma). MCF10A NLS copGFP and MCF10A paxillin-mCherry stable lines were prepared by lentiviral transduction using NLS copGFP pCDH and paxillin-mCherry pLV hygro tetOn plasmids, respectively. MCF10A F-tractin–EGFP (enhanced green fluorescent protein) stable lines were prepared using a transposon-based method with an F-tractin–EGFP plasmid. The backbone pPB puro tetOn was modified by swapping a eukaryotic antibiotic resistance marker from puromycin to zeocin. Then, the F-tractin–EGFP plasmid was prepared by inserting F-tractin–EGFP from F-tractin–EGFP C1 into pPB tetOn using Bam HI and Eco RI restriction sites. National Institutes of Health (NIH) 3T3 cells and GM00637 (Cornell Cell Repository) cells were cultured in DMEM supplemented with 10% fetal bovine serum (FBS; Thermo Fisher Scientific). PBMCs were cultured in RPMI (Thermo Fisher Scientific) supplemented with 1% GlutaMAX (Thermo Fisher Scientific) and 10% FBS (Thermo Fisher Scientific).

### Antibodies and reagents

The following antibodies were used: monoclonal FAK (13009S, Cell Signaling Technology); FAK$^{pY397}$ (8556S, Cell Signaling Technology); YAP (sc-101199, Santa Cruz Biotechnology); Ki-67 (9129S, Cell Signaling Technology). Alexa Fluor 647 anti-MHCII antibody (cz11, clone 130.8E8D9) was a gift of D. Antczak, Cornell University,

Ithaca, NY, USA. The FAK inhibitor was PF-573228 (5 μM; 14924, Cayman Chemical). The Src inhibitor was dasatinib (0.1 μM; 11498, Cayman Chemical).

### Cell morphology and spreading assays

MCF10A cells were plated on the PA and silicone gels at a density of 2600 cells/cm$^2$ and imaged after 24 hours with phase-contrast microscopy on an Olympus IX81 microscope with a 20× objective (0.40 NA; Zyla 4.2 sCMOS camera). Cell area was manually measured and analyzed with ImageJ.

### Cell proliferation assays

Cell proliferation was measured over a period of 4 days after seeding cells at an initial density of 2600 cells/cm$^2$. MCF10A NLS copGFP proliferation was continuously monitored by a custom epifluorescence microscope housed in a standard tissue culture incubator (37°C, 90% humidity, 5% $CO_2$; 10× objective; 1-hour acquisition intervals). Cell numbers were quantified manually every 24 hours using ImageJ. To measure cell viability, cells were seeded at a density of 1300 cells/cm$^2$ on fibronectin-functionalized PA and silicone gels in a 12-well plate and assayed after 24 hours with a LIVE/DEAD Viability/Cytotoxicity kit (Thermo Fisher Scientific). Fluorescence images were acquired using GFP and TXRED filter cubes on an Olympus IX81 microscope with a 10× objective (0.25 NA; Zyla 4.2 sCMOS camera) and quantified manually in ImageJ.

Cell proliferation analysis by assaying Ki-67 protein was done as follows: MCF10A cells were seeded at an initial density of 2600 cells/cm$^2$, cultured for 48 hours after seeding, and then fixed using 4% paraformaldehyde at room temperature for 30 min. Samples were incubated with Ki-67 primary antibody, followed by Alexa Fluor–conjugated secondary antibody. Nuclei were stained with Hoechst. The number of Ki-67–positive cells and total number of cells were counted manually with ImageJ.

### Gene expression analysis

Cells were grown on gels for 24 hours before harvesting with TRIzol (Invitrogen) for total RNA extraction. Power SYBR RNA-to-CT 1-Step Kit (4391178, Thermo Fisher Scientific) was used for reactions. The quantitative polymerase chain reaction (PCR) reactions were run with the ViiA 7 Real-Time PCR System and analyzed with QuantStudio Real-Time PCR Software. CTGF and ANKRD1 gene expression were calculated with the comparative $C_t$ method relative to glyceraldehyde-3-phosphate dehydrogenase (GAPDH). The primers used were ANKRD1 forward primer, AGTAGAGGAACTGGTCACTGG; ANKRD1 reverse primer, TGGGCTAGAAGTGTCTTCAGAT; CTGF forward primer, AGGAGTGGGTGTGTGACGA; CTGF reverse primer, CCAGGCAGTTGGCTCTAATC; GAPDH forward primer, CTGGGCTACACTGAGCACC; GAPDH reverse primer, AAGTGGTCGTTGAGGGCAATG.

### Isolation and culture of PBMCs

PBMCs were isolated from three thoroughbred horses: an 8-year-old gelding, a 12-year-old gelding, and an 18-year-old mare. The Institutional Animal Care and Use Committee (IACUC) of Cornell University approved the use of horses in these studies (IACUC no. 2018-0024). Blood (50 ml) was collected from the jugular vein using an 18-gauge needle and 60-ml syringe containing 5 ml of heparin (1000 U/ml; Sagent Pharmaceuticals), resulting in a final concentration of 100 U/ml of heparin. The blood was immediately stored on ice and transported to the laboratory for processing within 1 hour using Ficoll density gradient centrifugation (*50*). Briefly, freshly collected blood was diluted with equal volume of PBS containing 2% FBS (VWR Life Science Seradigm). A total of 20 ml of diluted blood was overlaid on 20-ml Ficoll-Paque PLUS (GE Healthcare, Chicago, IL) in a 50-ml conical tube. The Ficoll gradient centrifugation was performed at 400*g* for 30 min with low acceleration and no deceleration at room temperature. The PBMCs were collected from the plasma-Ficoll interface with a sterile Pasteur pipette and diluted 2:1 in PBS. After centrifugation at 300*g* for 5 min, the PBMCs pellet was resuspended in 10 ml of PBS and centrifuged at 300*g* for 5 min to wash the cells. The PBMCs were then cultured in RPMI supplemented with 1% GlutaMAX and 10% FBS.

### Preparation of a collagen master mix for 3D collagen I gels

To prepare a cell-free collagen I master mix of a defined volume (90 μl), 10 μl of a 10× concentrated minimal essential Eagle's medium (MEM) (M0275, Sigma-Aldrich) was added to 5 μl of a 7.5% sodium bicarbonate (BIC) solution (25080-060, Gibco) in a sterile tube and gently mixed until the indicator color changed from yellow (acidic) to purple (basic). Subsequently, 75 μl of purified bovine collagen I stock solution (3.0 mg/ml; PureCol) (5005-C, Advanced BioMatrix Inc.) was added to the MEM/BIC solution and gently mixed until a homogeneous, slightly purple color was obtained. The collagen I master mix was kept on ice for immediate use.

### PBMC-silicone interaction assay

The adherent fraction of isolated PBMCs was cultured for 4 to 5 days on tissue culture plastic with medium replacement every 1 to 2 days before experiments with silicones. Liquid silicone (SYLGARD 184, Dow Corning) was spread on the bottom of wells in a 96-well plate. Following an incubation time of 90 min at 70°C of the liquid silicone, cells (100,000 cells per well for 96-well plates) were seeded on top of the liquid silicone and allowed to adhere for 45 to 60 min at 37°C and 5% $CO_2$. Adherent cells were covered with a previously prepared collagen I master mix supplemented with cell culture medium to obtain a final concentration of 1.6 mg/ml. Polymerization of the collagen gel and equilibration of gas conditions within the collagen matrix took place for 20 to 30 min at 37°C and 5% $CO_2$ to obtain a final pH of 7.4 to 7.5. The pH values were determined using indicator paper strips. Cells attached to glass and silicone and covered with fibrillar collagen I matrices were maintained for 7 days with medium replacement every 1 to 2 days. For treating cells with inhibitors, dasatinib (11498, Cayman Chemical) and PF-573228 (14924, Cayman Chemical) were used at final concentrations of 0.1 and 5 μM, respectively, for 7 days.

### PBMC—silicone droplets interaction assay

PBMCs were cultured and used as described above. Silicone droplets containing media was prepared as follows: 100 μl of silicone liquid (SYLGARD 184, Dow Corning) was added to 3 ml of cell media into a 10-ml syringe barrel and further mixed by pushing and pulling the plunger in the barrel three times. Cells were embedded with silicone microdroplets in a 3D collagen I gel with a final concentration of 1.6 mg/ml. A total of 18,000 cells per condition were gently mixed with 22.5-μl silicone droplets containing media and added to 45 μl of the previously prepared collagen I master mix in a sterile tube on ice. The cell-containing collagen I solution was gently mixed until a homogeneous bright pink color was obtained

and subsequently transferred to a 96-well plate. Polymerization of the collagen gel and equilibration of gas conditions within the collagen matrix took place for 20 to 30 min at 37°C and 5% $CO_2$ to obtain a final pH of 7.4 to 7.5 (fig. S10B). The pH values were determined using indicator paper strips. Cells embedded in the silicone droplet containing collagen matrices were maintained for 3 days with medium replacement every 1 to 2 days.

### Immunofluorescence imaging

Cells were seeded at 5000 cells/cm$^2$ and fixed directly after 24 hours using 4% paraformaldehyde at room temperature for 30 min. For FAK inhibitor studies, 5000 cells/cm$^2$ were plated for 24 hours, serum-starved for 16 hours, treated with inhibitors for 2 hours, and stimulated with EGF (20 ng/ml) before fixation in 4% paraformaldehyde at room temperature. All samples were incubated with primary antibody, followed by Alexa Fluor–conjugated secondary antibodies. Nuclei were stained with Hoechst or through expression of NLS copGFP. Imaging was performed on a Zeiss LSM i880. Nuclear to cytoplasmic YAP signal was measured manually with ImageJ.

To prepare samples for immunofluorescence imaging in the PBMC-silicone/silicone droplets interaction assay, PBMCs were fixed with 4% paraformaldehyde at 4°C overnight, followed by staining with 1:5000 Hoechst, 1:200 Alexa Fluor 568 Phalloidin (Thermo Fisher Scientific), and 1:1000 Alexa Fluor 647 anti-MHCII antibody. Imaging was performed on a Zeiss LSM i800.

### Hertz contact model with surface tension

The contact problem is shown in fig. S6D. A rigid sphere with radius $R$ indents on a half space by its own weight. A buoyance-corrected gravitational force $F$ is applied on the substrate along the $z$ dimension, resulting in an indentation depth $d$ and a circular contact area with radius $a$.

The solution of this contact problem can be obtained using a recent work by Hui *et al.* (*28*). Let $a^*$ and $d^*$ denote the predicted contact radius and indentation depth for the classical Hertz model, which does not account for surface tension. For an incompressible elastic substrate with Young's modulus $E$, the apparent hardness $F/(a^*d^*)$ predicted by Hertz theory is

$$\frac{F}{a^* d^*} = \frac{16E}{9} \tag{1}$$

The result of Hui *et al.* predicts that the hardness, corrected for surface tension, is

$$\frac{F}{ad} = \frac{16E}{9}\overline{P_H}\left(\frac{3}{2\omega}\right) \tag{2}$$

where $\overline{P_H}\left(\frac{3}{2\omega}\right)$ is the dimensionless function

$$\overline{P_H}\left(\frac{3}{2\omega}\right) = 1 + \frac{9\pi}{8\omega}\left[\frac{\left(\frac{3}{2\omega}\right)^2 + 0.6016\left(\frac{3}{2\omega}\right) + 0.0171}{\left(\frac{3}{2\omega}\right)^2 + 0.3705\left(\frac{3}{2\omega}\right) + 0.0063}\right] \tag{3}$$

which depends only on the elastocapillary number

$$\omega = \frac{a \cdot E}{\gamma} \tag{4}$$

where $\gamma$ is the surface tension. The function $\overline{P_H}\left(\frac{3}{2\omega}\right)$ is a correction term that compensates for surface tension. For example, for small elastocapillary number, $\frac{3}{2\omega} \to 0$, surface tension effect becomes insignificant; $\overline{P_H}\left(\frac{3}{2\omega}\right)$ goes to one, and $a^*d^* = ad$. Specifically, the ratio of the observed and Hertz or apparent hardness is obtained by dividing Eq. 2 by Eq. 1. This results in

$$\frac{a^* d^*}{ad} = \overline{P_H}\left(\frac{3}{2\omega}\right) \tag{5}$$

The apparent hardness given by Eq. 1 can be computed using the buoyance-corrected gravitational force and the modulus of substrate. Using Eq. 5 above, fig. S6D plots the ratio of observed to predicted hardness, $a^*d^*/ad$, versus the elastocapillary number, $a{\cdot}E/\gamma$.

### Statistics

Differences in FAK activation on reported substrates were tested for normality using a Shapiro-Wilk goodness-of-fit test and for equal variances using a Levene's test. If model assumptions were met, then data were analyzed by one-way analysis of variance (ANOVA) with Tukey's post hoc tests, with $\alpha = 0.05$. A Wilcoxon rank scores test was used to analyze data that did not meet model assumptions. The analyses were performed in JMP Pro 14 statistical software (SAS Institute, Cary, NC). Statistical significance for all other experiments was determined by Student's $t$ test and one-way ANOVA using GraphPad Prism, as appropriate.

## SUPPLEMENTARY MATERIALS

Supplementary material for this article is available at http://advances.sciencemag.org/cgi/content/full/6/15/eaay0076/DC1

View/request a protocol for this paper from *Bio-protocol*.

## REFERENCES AND NOTES


1. G. M. Whitesides, E. Ostuni, S. Takayama, X. Jiang, D. E. Ingber, Soft lithography in biology and biochemistry. *Annu. Rev. Biomed. Eng.* **3**, 335–373 (2001).
2. E. Gutierrez, E. Tkachenko, A. Besser, P. Sundd, K. Ley, G. Danuser, M. H. Ginsberg, A. Groisman, High refractive index silicone gels for simultaneous total internal reflection fluorescence and traction force microscopy of adherent cells. *PLOS ONE* **6**, e23807 (2011).
3. S. Kuddannaya, Y. J. Chuah, M. H. A. Lee, N. V. Menon, Y. Kang, Y. Zhang, Surface chemical modification of poly(dimethylsiloxane) for the enhanced adhesion and proliferation of mesenchymal stem cells. *ACS Appl. Mater. Interfaces* **5**, 9777–9784 (2013).
4. L. Keith, W. Herlihy, H. Holmes, P. Pin, Breast implant–associated anaplastic large cell lymphoma. *Proc. Bayl. Univ. Med. Cent.* **30**, 441–442 (2017).
5. L. S. Nichter, M. A. Mueller, R. G. Burns, J. M. Stallman, First report of nodal marginal zone B-cell lymphoma associated with breast implants. *Plast. Reconstr. Surg.* **129**, 576e–578e (2012).
6. W. Siggelkow, A. Faridi, K. Spiritus, U. Klinge, W. Rath, B. Klosterhalfen, Histological analysis of silicone breast implant capsules and correlation with capsular contracture. *Biomaterials* **24**, 1101–1109 (2003).
7. E. D. Austad, Breast implant-related silicone granulomas: The literature and the litigation. *Plast. Reconstr. Surg.* **109**, 1724–1730 (2002).
8. N. Handel, M. E. Garcia, R. Wixtrom, Breast implant rupture: Causes, incidence, clinical impact, and management. *Plast. Reconstr. Surg.* **132**, 1128–1137 (2013).
9. S. Makwana, B. Basu, Y. Makasana, A. Dharamsi, Prefilled syringes: An innovation in parenteral packaging. *Int. J. Pharm. Investig.* **1**, 200–206 (2011).
10. J. H. Yu, E. Gallemore, J. K. Kim, R. Patel, J. Calderon, R. P. Gallemore, Silicone oil droplets following intravitreal bevacizumab injections. *Am. J. Ophthalmol. Case Rep.* **10**, 142–144 (2018).
11. L. Liu, T. W. Randolph, J. F. Carpenter, Particles shed from syringe filters and their effects on agitation-induced protein aggregation. *J. Pharm. Sci.* **101**, 2952–2959 (2012).
12. E. Chantelau, M. Berger, B. Böhlken, Silicone oil released from disposable insulin syringes. *Diabetes Care* **9**, 672–673 (1986).
13. J. M. Lee, Y. J. Kim, Foreign body granulomas after the use of dermal fillers: Pathophysiology, clinical appearance, histologic features, and treatment. *Arch. Plast. Surg.* **42**, 232–239 (2015).
14. T. Yeung, P. C. Georges, L. A. Flanagan, B. Marg, M. Ortiz, M. Funaki, N. Zahir, W. Ming, V. Weaver, P. A. Janmey, Effects of substrate stiffness on cell morphology, cytoskeletal structure, and adhesion. *Cell Motil. Cytoskeleton* **60**, 24–34 (2005).

15. M. J. Paszek, N. Zahir, K. R. Johnson, J. N. Lakins, G. I. Rozenberg, A. Gefen, C. A. Reinhart-King, S. S. Margulies, M. Dembo, D. Boettiger, D. A. Hammer, V. M. Weaver, Tensional homeostasis and the malignant phenotype. *Cancer Cell* **8**, 241–254 (2005).
16. A. J. Engler, S. Sen, H. L. Sweeney, D. E. Discher, Matrix elasticity directs stem cell lineage specification. *Cell* **126**, 677–689 (2006).
17. R. J. Pelham Jr, Y. I. Wang, Cell locomotion and focal adhesions are regulated by substrate flexibility. *Proc. Natl. Acad. Sci. U.S.A.* **94**, 13661–13665 (1997).
18. B. Geiger, J. P. Spatz, A. D. Bershadsky, Environmental sensing through focal adhesions. *Nat. Rev. Mol. Cell Biol.* **10**, 21–33 (2009).
19. O. Chaudhuri, L. Gu, M. Darnell, D. Klumpers, S. A. Bencherif, J. C. Weaver, N. Huebsch, D. J. Mooney, Substrate stress relaxation regulates cell spreading. *Nat. Commun.* **6**, 6365 (2015).
20. O. Chaudhuri, L. Gu, D. Klumpers, M. Darnell, S. A. Bencherif, J. C. Weaver, N. Huebsch, H.-p. Lee, E. Lippens, G. N. Duda, D. J. Mooney, Hydrogels with tunable stress relaxation regulate stem cell fate and activity. *Nat. Mater.* **15**, 326–334 (2016).
21. M. J. Paszek, V. M. Weaver, The tension mounts: Mechanics meets morphogenesis and malignancy. *J. Mammary Gland Biol. Neoplasia* **9**, 325–342 (2004).
22. M. L. Previtera, A. Sengupta, Substrate stiffness regulates proinflammatory mediator production through TLR4 activity in macrophages. *PLOS ONE* **10**, e0145813 (2015).
23. A. K. Blakney, M. D. Swartzlander, S. J. Bryant, The effects of substrate stiffness on the in vitro activation of macrophages and in vivo host response to poly(ethylene glycol)-based hydrogels. *J. Biomed. Mater. Res. A* **100**, 1375–1386 (2012).
24. S. Ishihara, M. Yasuda, I. Harada, T. Mizutani, K. Kawabata, H. Haga, Substrate stiffness regulates temporary NF-κB activation via actomyosin contractions. *Exp. Cell Res.* **319**, 2916–2927 (2013).
25. K. R. Levental, H. Yu, L. Kass, J. N. Lakins, M. Egeblad, J. T. Erler, S. F. T. Fong, K. Csiszar, A. Giaccia, W. Weninger, M. Yamauchi, D. L. Gasser, V. M. Weaver, Matrix crosslinking forces tumor progression by enhancing integrin signaling. *Cell* **139**, 891–906 (2009).
26. P. Lu, V. M. Weaver, Z. Werb, The extracellular matrix: A dynamic niche in cancer progression. *J. Cell Biol.* **196**, 395–406 (2012).
27. M. W. Pickup, J. K. Mouw, V. M. Weaver, The extracellular matrix modulates the hallmarks of cancer. *EMBO Rep.* **15**, 1243–1253 (2014).
28. C.-Y. Hui, T. Liu, T. Salez, E. Raphael, A. Jagota, Indentation of a rigid sphere into an elastic substrate with surface tension and adhesion. *Proc Math. Phys. Eng. Sci.* **471**, 20140727 (2015).
29. R. W. Style, C. Hyland, R. Boltyanskiy, J. S. Wettlaufer, E. R. Dufresne, Surface tension and contact with soft elastic solids. *Nat. Commun.* **4**, 2728 (2013).
30. X. Xu, A. Jagota, C.-Y. Hui, Effects of surface tension on the adhesive contact of a rigid sphere to a compliant substrate. *Soft Matter* **10**, 4625–4632 (2014).
31. G. P. Maxwell, A. Gabriel, Breast implant design. *Gland Surg.* **6**, 148–153 (2017).
32. X. Q. Brown, K. Ookawa, J. Y. Wong, Evaluation of polydimethylsiloxane scaffolds with physiologically-relevant elastic moduli: Interplay of substrate mechanics and surface chemistry effects on vascular smooth muscle cell response. *Biomaterials* **26**, 3123–3129 (2005).
33. T. Boudou, J. Ohayon, C. Picart, P. Tracqui, An extended relationship for the characterization of Young's modulus and Poisson's ratio of tunable polyacrylamide gels. *Biorheology* **43**, 721–728 (2006).
34. C. M. Cesa, N. Kirchgessner, D. Mayer, U. S. Schwarz, B. Hoffmann, R. Merkel, Micropatterned silicone elastomer substrates for high resolution analysis of cellular force patterns. *Rev. Sci. Instrum.* **78**, 034301 (2007).
35. S. Dupont, L. Morsut, M. Aragona, E. Enzo, S. Giulitti, M. Cordenonsi, F. Zanconato, J. Le Digabel, M. Forcato, S. Bicciato, N. Elvassore, S. Piccolo, Role of YAP/TAZ in mechanotransduction. *Nature* **474**, 179–183 (2011).
36. N.-G. Kim, B. M. Gumbiner, Adhesion to fibronectin regulates Hippo signaling via the FAK–Src–PI3K pathway. *J. Cell Biol.* **210**, 503–515 (2015).
37. H. Hertz, Ueber die Berührung fester elastischer Körper. *J. Für Reine Angew. Math.* **92**, 156–171 (1882).
38. J. M. Long, G. F. Wang, Effects of surface tension on axisymmetric Hertzian contact problem. *Mech. Mater.* **56**, 65–70 (2013).
39. A. R. Cameron, J. E. Frith, J. J. Cooper-White, The influence of substrate creep on mesenchymal stem cell behaviour and phenotype. *Biomaterials* **32**, 5979–5993 (2011).
40. A. R. Cameron, J. E. Frith, G. A. Gomez, A. S. Yap, J. J. Cooper-White, The effect of time-dependent deformation of viscoelastic hydrogels on myogenic induction and Rac1 activity in mesenchymal stem cells. *Biomaterials* **35**, 1857–1868 (2014).
41. B. Trappmann, J. E. Gautrot, J. T. Connelly, D. G. T. Strange, Y. Li, M. L. Oyen, M. A. Cohen Stuart, H. Boehm, B. Li, V. Vogel, J. P. Spatz, F. M. Watt, W. T. S. Huck, Extracellular-matrix tethering regulates stem-cell fate. *Nat. Mater.* **11**, 642–649 (2012).
42. J. G. Evans, I. Correia, O. Krasavina, N. Watson, P. Matsudaira, Macrophage podosomes assemble at the leading lamella by growth and fragmentation. *J. Cell Biol.* **161**, 697–705 (2003).
43. J. M. Anderson, A. Rodriguez, D. T. Chang, Foreign body reaction to biomaterials. *Semin. Immunol.* **20**, 86–100 (2008).
44. S. Chen, J. A. Jones, Y. Xu, H.-Y. Low, J. M. Anderson, K. W. Leong, Characterization of topographical effects on macrophage behavior in a foreign body response model. *Biomaterials* **31**, 3479–3491 (2010).
45. A. Engler, L. Bacakova, C. Newman, A. Hategan, M. Griffin, D. Discher, Substrate compliance versus ligand density in cell on gel responses. *Biophys. J.* **86**, 617–628 (2004).
46. J. H. Wen, L. G. Vincent, A. Fuhrmann, Y. S. Choi, K. C. Hribar, H. Taylor-Weiner, S. Chen, A. J. Engler, Interplay of matrix stiffness and protein tethering in stem cell differentiation. *Nat. Mater.* **13**, 979–987 (2014).
47. F. Bordeleau, B. N. Mason, E. M. Lollis, M. Mazzola, M. R. Zanotelli, S. Somasegar, J. P. Califano, C. Montague, D. J. LaValley, J. Huynh, N. Mencia-Trinchant, Y. L. N. Abril, D. C. Hassane, L. J. Bonassar, J. T. Butcher, R. S. Weiss, C. A. Reinhart-King, Matrix stiffening promotes a tumor vasculature phenotype. *Proc. Natl. Acad. Sci. U.S.A.* **114**, 492–497 (2017).
48. J. N. Lakins, A. R. Chin, V. M. Weaver, Exploring the link between human embryonic stem cell organization and fate using tension-calibrated extracellular matrix functionalized polyacrylamide gels. *Methods Mol. Biol* **916**, 317–350 (2012).
49. P. Erni, P. Fischer, E. J. Windhab, V. Kusnezov, H. Stettin, J. Läuger, Stress- and strain-controlled measurements of interfacial shear viscosity and viscoelasticity at liquid/liquid and gas/liquid interfaces. *Rev. Sci. Instrum.* **74**, 4916–4924 (2003).
50. C. McGuckin, M. Jurga, H. Ali, M. Strbad, N. Forraz, Culture of embryonic-like stem cells from human umbilical cord blood and onward differentiation to neural cells *in vitro*. *Nat. Protoc.* **3**, 1046–1055 (2008).


**Acknowledgments:** We thank J. Felippe for the antibody to equine MHCII, J. Lammerding for NLS copGFP pCDH plasmid, V. Weaver and J. Lakins for Paxillin-mCherry pLV hygro tetOn and pPB puro tetOn plasmids, and C. Waterman for the F-tractin-EGFP C1 plasmid. We thank M. Colville for assistance with cloning and microscopy. **Funding:** This investigation was supported by the NIH under Ruth L. Kirschstein National Research Service Award (2T32GM008267) from the National Institute of General Medical Sciences (C.R.S.), the Knight Family Foundation Graduate Research Fellowship in Nanoscience and Technology (C.R.S.), Samuel C. Fleming Family Graduate Fellowship (Z.C. and C.R.S.), Kavli Institute at Cornell Postdoctoral fellowship (S.S.), National Institute of Arthritis and Musculoskeletal and Skin Diseases K08AR068469 (H.L.R.), National Cancer Institute R33-CA193043 and U54 CA210184 (M.J.P.), and Division of Materials Sciences and Engineering Sciences, Office of Basic Energy Sciences, U.S. Department of Energy DEFG02-07ER46463 (C.-Y.H.). Confocal imaging was supported through the Cornell University Biotechnology Resource Center (BRC) Imaging Facility (grant NIH S10OD018516). This work made use of the Cornell NanoScale Facility, a member of the National Nanotechnology Coordinated Infrastructure (NNCI; NSF grant ECCS-1542081). This work also made use of the Cornell Center for Materials Research Shared Facilities (NSF MRSEC program DMR-1120296). **Author contributions:** All authors contributed to the results and the final preparation of the manuscript. Z.C., C.R.S., S.S., J.A.S., C.-Y.H., H.L.R., and M.J.P. conceived and designed the experimental plan. Z.C. and V.K.G. conducted the bulk mechanical testing. A.S. conducted the interfacial rheology measurements. Z.C. conducted the focal adhesion and YAP/TAZ imaging experiments and the proliferation and viability studies. C.R.S. and G.C. conducted the gene expression experiments. A.R.W. and J.S. collected equine blood and harvested primary monocytes. Z.C. and S.S. conducted collagen overlay and 3D culture assays. **Competing interests:** The authors declare that they have no competing interests. **Data and materials availability:** All data needed to evaluate the conclusions in the paper are present in the paper and/or the Supplementary Materials. Additional raw data and plasmids related to this paper may be requested from the authors.

Submitted 15 May 2019
Accepted 8 January 2020
Published 10 April 2020
10.1126/sciadv.aay0076

**Citation:** Z. Cheng, C. R. Shurer, S. Schmidt, V. K. Gupta, G. Chuang, J. Su, A. R. Watkins, A. Shetty, J. A. Spector, C.-Y. Hui, H. L. Reesink, M. J. Paszek, The surface stress of biomedical silicones is a stimulant of cellular response. *Sci. Adv.* **6**, eaay0076 (2020).